Faraday Discussions

Accepted Manuscript

This manuscript will be presented and discussed at a forthcoming Faraday Discussion meeting. All delegates can contribute to the discussion which will be included in the final volume.

Register now to attend! Full details of all upcoming meetings: http://rsc.li/fd-upcoming-meetings

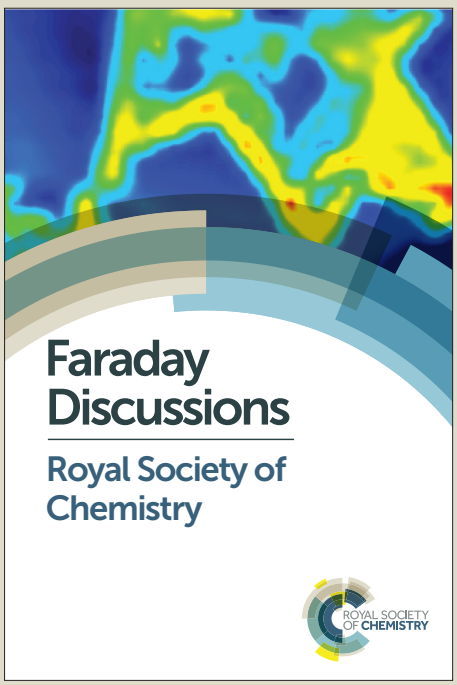

This is an *Accepted Manuscript*, which has been through the Royal Society of Chemistry peer review process and has been accepted for publication.

Accepted Manuscripts are published online shortly after acceptance, before technical editing, formatting and proof reading. Using this free service, authors can make their results available to the community, in citable form, before we publish the edited article. We will replace this *Accepted Manuscript* with the edited and formatted *Advance Article* as soon as it is available.

You can find more information about *Accepted Manuscripts* in the Information for Authors.

Please note that technical editing may introduce minor changes to the text and/or graphics, which may alter content. The journal's standard Terms & Conditions and the Ethical guidelines still apply. In no event shall the Royal Society of Chemistry be held responsible for any errors or omissions in this *Accepted Manuscript* or any consequences arising from the use of any information it contains.

ROYAL SOCIETY OF CHEMISTRY

www.rsc.org/faraday_d

Aqueous Solution/Metal Interfaces Investigated *in operando* by Photoelectron Spectroscopy

O. Karslıoğlu[a], S. Nemsak[b], I. Zegkinoglou[a,#], A. Shavorskiy[a,§], M. Hartl[a,c], F. Salmassi[d], E.M. Gullikson[d], M.L. Ng[e], Ch. Rameshan[a,$], B. Rude[a], D. Bianculli[i], A.A. Cordones[a], S. Axnanda[f,&], E.J. Crumlin[f], P.N. Ross[d], C.M. Schneider[b], Z. Hussain[f], Z. Liu[f,g,*], C.S. Fadley[d,h,*], H. Bluhm[a,*]

[a] *Chemical Sciences Division, Lawrence Berkeley National Laboratory, Berkeley, CA 94720.*
[b] *Peter-Grünberg-Institut PGI-6, Forschungszentrum Jülich GmbH, 52425 Jülich, Germany.*
[c] *Julius -Maximilians-Universität Würzburg, Sanderring 2, 97070 Würzburg, Germany.*
[d] *Materials Sciences Division, Lawrence Berkeley National Laboratory, Berkeley, CA 94720.*
[e] *SLAC National Accelerator Laboratory, 2575 Sand Hill Road, Menlo Park, CA 94025.*
[f] *Advanced Light Source, Lawrence Berkeley National Laboratory, Berkeley, CA 94720.*
[g] *State Key Laboratory of Functional Materials for Informatics, Shanghai Institute of Microsystem and Information Technology, Chinese Academy of Sciences, Shanghai 200050.*
[h] *Department of Physics, University of California Davis, Davis, CA 95616.*
[i] *Engineering Division, Lawrence Berkeley National Laboratory, Berkeley, CA 94720.*

Abstract

We describe a new *in operando* approach for the investigation of heterogeneous processes at solid/liquid interfaces with elemental and chemical specificity which combines the preparation of thin liquid films using the meniscus method with standing wave ambient pressure X-ray photoelectron spectroscopy (Nemšák et al., Nature Communications **5**, 5441 (2014)). This technique provides information about the chemical composition across liquid/solid interfaces with sub-nanometer depth resolution and under realistic conditions of solution composition and concentration, pH, as well as electrical bias. In this article, we discuss the basics of the technique and present first results of measurements on KOH/Ni interfaces.

Keywords: Ambient pressure X-ray photoelectron spectroscopy, standing wave photoemission spectroscopy, liquid/solid interfaces

---

* Corresponding authors: E-mails: ZLiu2@lbl.gov, CSFadley@ucdavis.edu, HBluhm@lbl.gov.

[#] Present address: Lehrstuhl für Experimentalphysik IV, Ruhr-Universität Bochum, D-44780 Bochum, Germany.

[§] Present address: MAX IV Laboratory, Lund University, P.O. Box 118, SE-221 00 Lund, Sweden.

[&] Present address: BASF Catalysts LLC, 25 Middlesex Avenue, Iselin, NJ 08830.

[$] Present address: Vienna University of Technology, Institute of Materials Chemistry, 1060 Vienna, Austria.

Introduction

Liquid/solid and gas/solid interfaces govern the majority of reactions in corrosion science. Metals undergo changes to their surface under atmospheric conditions, when thin aqueous layers are condensed on their surface, or when they are immersed in a bulk solution. Corrosion is inherently an electrochemical process and is characterized by a concurrent transfer of mass and charge across the metal/solution interface in a coupled electrochemical reaction, where anodic and cathodic processes occur simultaneously either at different sites on the same material or on different parts of the system.[1] The transfer of metal atoms into solution through oxidation in the anodic reaction leads to the structural weakening of the material and can ultimately result in mechanical failure, with potentially dire consequences.

A detailed understanding of the processes governing corrosion requires the investigation of the metal surface in interaction with its surrounding gas-phase or liquid-phase environment on the atomic scale. Surface science investigations into corrosion processes can be performed in principle in two ways, either by comparing the state of the surface before and after the corrosion process has taken place (*i.e.*, *ex situ*), or *in operando*, *i.e.* monitoring the surface during the process. While the whole arsenal of surface science methods can be used to perform *ex situ* investigations, the use of *in operando* methods often poses experimental challenges. These include the need to operate under elevated pressure conditions, since the partial pressure of water and aqueous solutions at environmental temperatures ranges from some tenths of Torr to tens of Torr. Another challenge is enhancing the signal from the interface region over that originating from the bulk liquid and solid. Over the past decades, considerable progress has been made in the adaptation of vacuum-based surface science techniques to investigations of surfaces under realistic relative humidity and even liquid/solid interfaces. Surface sensitive spectroscopies that can be used under these conditions include optical methods, such as infrared spectroscopy (IR)[2,3] and vibrational sum-frequency generation (VSFG)[4,5]; X-ray emission spectroscopy (XES)[6]; near edge X-ray absorption fine structure (NEXAFS) with fluorescence detection[7] as well as surface X-ray diffraction (SXRD)[8]. Among the imaging techniques that can be used to study surfaces in the presence of gases and liquids are scanning force microscopy (SFM) in both contact[9] and non-contact[10] modes, as well as scanning tunneling microscopy (STM)[11], and in recent years also transmission electron microscopy (TEM)[12] and scanning electron microscopy (SEM)[13]. A recent overview of surface science techniques used for measuring liquid/solid interfaces is given in Ref. 14.

X-ray photoelectron spectroscopy (XPS) is an excellent method for monitoring corrosion processes, since it is exquisitely surface sensitive due to the short mean free path of electrons in

matter at the typical kinetic energies (KE) used in XPS (a few 100 to a few 1000 eV). XPS permits quantitatively determining the elemental composition of the surface and, through detection of so called "chemical shifts", also the oxidation states of the different components of the surface. Since XPS uses electrons as probes, changes in local electrical potentials can also be monitored as they will lead to rigid kinetic energy shifts experienced by all core level and valence peaks and can thus be distinguished from shifts due to chemical changes.[15] XPS is thus ideally suited to study corrosion processes since it permits monitoring both changes in the chemistry as well as electronic properties of the surface simultaneously and in non-contact.

However, corrosion processes commonly take place under ambient conditions around room temperature and with an equilibrium water vapor pressure. At higher pressures, the scattering of electrons by gas molecules and the risk of arcing in the electrostatic lens or the detector pose serious problems. These limitations have been overcome through ambient pressure X-ray photoelectron spectroscopy (APXPS), which combines all advantages of vacuum-based XPS – quantitative elemental and chemical information at high surface sensitivity – with the possibility to measure samples at elevated pressures.[16,17,18] The technique was first introduced by the Siegbahn group in Uppsala/Sweden in the early 1970s. These spectrometers used several differential pumping stages between the sample cell and the hemispherical electron analyzer, with a small entrance aperture to the first pumping stage brought into close vicinity of the sample surface, to both minimize the path length of the electrons through the high pressure region and the leakage of gas into the spectrometer. The inelastic mean free path (IMFP) of electrons with a kinetic energy of 100 eV (*i.e.*, those with the highest surface sensitivity) is about 1 mm in 1 Torr of water vapor. Typical distances between the sample and the entrance aperture are ~1 mm. APXPS was further developed in the late 1990s by introducing electrostatic lenses in the differential pumping stages which overcame the tradeoff between collection angle for electron detection and maximum pumping efficiency. A schematic layout of such a system is shown in Fig. 1. These instruments can now operate at pressures above 20 Torr, thus passing the important threshold of the equilibrium vapor pressures of water at room temperature. As an illustrative example of the importance of pressure, recent APXPS studies of Cu surfaces have shown the importance of the surface crystallography for the wettability of metals: While Cu(110) is covered by a mixed hydroxyl/water layer at a relative humidity (RH) of 5 %, Cu(111) does not react with water vapor at the same RH, due to the higher dissociation barrier of water on the less reactive (111) surface.[19,20] From these data and other studies of surfaces under ambient RH[21,22] a picture emerges in which most oxide and metal surfaces are hydroxylated and show adsorbed molecular water at relative humidities far below those present under normal ambient conditions, with

significant consequences for atmospheric corrosion processes on metals.

While the investigation of solid/vapor interfaces at relevant relative humidities with high chemical and surface sensitivity using APXPS has become a standard method over the past decade, the investigation of solid/liquid interfaces using photoelectron spectroscopy is still a challenging task. Kolb *et al*. developed a quasi-*in situ* method for determining the composition and charge state of electrochemical interfaces using UHV XPS combined with an electrochemical cell in which the sample surface was dipped into an aqueous solution under potential, then removed, dried and transferred to the XPS measurement chamber.[23] Even though most of the water evaporated from the interface, the electrical double layer (EDL) was shown to be preserved so that measurements of the potential drop in the EDL became possible.[24,25] While this method has been proven to be a viable strategy for the investigation of the static properties of the EDL, it is not suitable for studies of corrosion processes *in operando* due to the lack of charge and mass transport during the XPS measurements. Artifacts can also result from the drying of the surface. True *in operando* measurements require the presence of a thicker solution layer in contact with a solution reservoir at the interface.

Since electrons are strongly scattered by ions and molecules in a liquid, there is a limit to the thickness of the solution layer in normal XPS measurements. Figure 2 presents calculated and measured data of the inelastic mean free path of electrons in liquid water.[26] For maximum achievable kinetic energies in experiments using an Al Kα lab source (1486.7 eV) the IMFP is only about 6 nm, or 20 water monolayers. Recent developments of high KE APXPS instruments have opened the opportunity to detect electrons with much higher KE.[27] For a Cu Kα source (8047.8 eV) or a hard X-ray beamline at a synchrotron with 8 keV incident photon energy, 8 keV electrons with an IMFP of ~20 nm in liquid water can be detected. One can argue that at these water film thicknesses the properties of the liquid/solid interface approach or are that of a true bulk liquid/solid interface.

For the study of solid/liquid interfaces with stable liquid layers of a thickness between several nm and several 10 nm, XPS measurements of all core levels of interest with sufficient signal-to-noise ratios are complicated by the expected low signal from the interface due to the attenuation of the electrons in the gas as well as liquid phase. One intriguing approach to preparing liquid layers with thicknesses in the nm range is the adaptation of the well-established liquid jet method, which has been successfully used to measure the composition of liquid/vapor interfaces.[28] For the investigation of liquid/solid interfaces, liquid jets are prepared from solutions containing suspended nanoparticles, where some of the nanoparticles reside sufficiently close to the surface of the liquid jet so that their interface with the solution can be probed using XPS.[29]

This method has been successfully used to investigate, e.g., the surface charge density of silica particles as a function of particle size and pH of the solution, but has not yet been tested for its applicability to corrosion studies.[29]

Another recently explored method to measure liquid/solid interfaces is the detection of photoelectrons through a thin membrane (e.g., multilayer graphene), with the photoelectron analyzer located on the vacuum side of the membrane.[30] The advantage of this approach is that it overcomes the need for a thin solution layer in XPS investigations of the liquid/solid interface. The challenge here is to prepare ultrathin solid films of the material of interest so that photoelectrons can penetrate the solid on their way to the detector, as well as the enhancement of the interface signal over that from the bulk, which is in fact closer to the spectrometer. Also, this method does not lend itself to a standing wave approach as described below.

A further possibility to prepare thin liquid films is to expose the sample to precisely controlled relative humidities just below saturation (RH 100 %), since the water film thickness increases rapidly as the RH approaches 100 %. The challenges of this approach are three-fold: (I) The precise control of temperature and water vapor pressure in the experiment, since any small deviation will lead to rapid liquid film growth or desorption. (II) The control of the concentration and pH of the solution. While alkali halide solution films have successfully been formed by re-hydrating either drop-cast or evaporated alkali halide films inside a humidity-controlled vacuum chamber[31,32], the exact control of the concentration and pH of the film is challenging. (III) Finally, the connection of the liquid film to an external electrical circuit, which might be achieved using an approach akin to scanning probe methods to immerse an electrode into the thin solution film.

These challenges can be overcome using the so-called meniscus method, which was first introduced many decades ago by Bockris and colleagues for the determination of the dissolution of gases in porous electrodes[33], and recently been applied by some of the authors of this article for the first time to studies of liquid/solid interfaces using APXPS.[27] The principle is shown in Fig. 3. The sample is immersed in a solution inside the measurement cell and can then be electrochemically cleaned of hydrocarbons and other contamination. When it is partially withdrawn from the solution, a meniscus will extend to a height z_1 (for neat water on a hydrophilic surface, a few mm)[34] above the bulk solution surface. Under favorable conditions and in the presence of a vapor pressure p_{vap} (which is a function of the solution temperature T_{sol}) close to saturation, a thin liquid film can be stabilized over the whole range over which the sample was originally dipped into the solution (z_2). Close to the top of the liquid film (at ~z_2) parts of the liquid film are sufficiently thin to allow collection of photoelectron spectra from the liquid/solution interface. Liquid films formed in that manner have been shown to be stable for

many hours.[27] This method was used in the present experiments and is described in more detail in the Experimental section.

The last challenge that needs to be overcome in the study of liquid/solid interfaces using APXPS is enhancing the signal from the narrow interfacial region over that originating from the bulk of the liquid layer and solid substrate. To that end, some of the authors of this paper have recently introduced standing wave ambient pressure photoemission spectroscopy (SWAPPS), which is based on well-established standing wave photoemission spectroscopy, where the exciting X-ray wave field is tailored into a standing wave that is scanned through the interface of interest and thus provides much increased depth-resolution in XPS experiments (see Fig. 4).[35,36] The advantage of the standing wave approach is that it provides a built-in ruler, *i.e.*, the period of the standing wave, to determine absolute depth distributions of chemical species throughout the probed volume. The combination of SWAPPS with the meniscus method for the preparation of thin liquid layers thus has the potential to provide detailed chemical information about all components of the system (bulk liquid, liquid/solid interface, bulk solid) with sub-nm resolution in the direction perpendicular to the interface, with full control over the concentration and pH of the solution, as well as the applied potentials. In the following we describe the experimental details and present a proof-of-principle investigation for the reaction of Ni immersed in a 0.1 M KOH solution under oxidizing conditions.

Experimental

Preparation of thin liquid films

Figure 3 describes the experimental setup used in the current investigations. A glass beaker (outer diameter 3.2 cm, height 5 cm) is mounted inside a vacuum chamber using an UltraTorr (O-ring seal) fitting. A Ag/AgCl reference electrode (eDAQ, leakless miniature) is glued into a hole in the bottom of the beaker. A Pt counter electrode is fused into the bottom of the glass beaker. The UltraTorr fitting is attached via an XYZ manipulation stage to the bottom flange of a high-vacuum chamber, which in turn is mounted to the front end of the differentially pumped electron lens system of the APXPS spectrometer. The sample is mounted on an XYZ manipulator and a rotational stage. A commercial KOH solution (Alfa Aesar, 30% w/v) is diluted to 0.1 M with ultra-pure water, and then degassed in a separate chamber by pumping before being introduced into the beaker inside the experimental cell. The solution temperature T_{sol} is allowed to equilibrate to the temperature of the surrounding parts of the experiment and not actively controlled. The experimental cell is slowly evacuated using an external roughing pump until the pressure in the cell, measured using a capacitance pressure gauge, is close to that of the expected

vapor pressure of the solution at room temperature (p_{vap}), at which point the external pump is isolated. During the experiments the measurement cell is pumped through the front aperture (diameter 0.1 mm) of the differentially pumped electrostatic lens; the loss in gas molecules in the experimental cell is compensated for by evaporation from the solution in the beaker, and from a separate water reservoir (~5 cm^3; not shown) that acts as a buffer to reduce the decrease of the solution level in the beaker and limit the change in solution temperature due to evaporative cooling. With this procedure experiments can be performed up to 24 hours without the necessity to refill the beaker with fresh solution, and with only minor changes in the solution concentration.

At the beginning of the experiment the sample is immersed as far as possible into the solution and its electrochemical properties are characterized (see Fig. 5c) using a Bio-Logic SP-150 potentiostat. By using appropriate parameters for cyclic voltammograms (CV), the sample surface can also be cleaned, e.g., from carbon contamination. When the sample is then partially retracted from the solution, a meniscus forms, which – for a hydrophilic sample – extends to a height z_1 above the bulk liquid surface (see Figure 3), with z_1 being close to the capillary length, which is of the order of a few mm for water.[34] A thin, continuous solution film extends beyond the meniscus up to a height z_2, the depth to which the sample was originally immersed into the solution. This film is in electrical contact with the solution in the beaker, confirmed by shifts in the photoelectron peaks of the thin film upon application of a bias to the solution in the beaker. The film is stabilized by the high RH (in case of an aqueous solution) close to 100 % due to the presence of the vapor pressure above the solution. The initial, electrochemical removal of hydrophobic contaminations also supports the formation of a continuous liquid film. Above the height z_2 there is also water adsorption (from the gas phase), but these parts of the liquid film are usually not in electrical contact with the solution in the beaker, most likely due to hydrophobic contamination which prevents the formation of a continuous film. In some cases the thin water film between z_1 and z_2 breaks up and forms areas where patches of electrolyte remain with the thickness and ion concentration of the continuous film, but without electrical contact to the solution in the beaker. A photograph of the sample in the measurement position is shown in Figure 5b.

We note that a similar approach for the preparation of a thin film has also been used to study the interface between an ionic liquid (vapor pressure $<10^{-9}$ Torr) and a metal electrode, where the sample was not in a vertical position but only slightly tilted out of the horizontal direction.[37]

Multilayer sample preparation

A Si/Mo multilayer was prepared on a Si(100) substrate at the Lawrence Berkeley National

Laboratory Center for X-ray Optics. The multilayer mirror consists of 80 repeats of a Si 1.5 nm/Mo 1.9 nm bilayer, yielding a multilayer periodicity of 3.4 nm. The setup of the sample is shown in Fig. 4. A cap layer of 1.3 nm of SiO_2 terminates the mirror. A Ni layer with a thickness of ~8 nm was grown on the SiO_2 cap layer using magnetron sputtering in an ultrahigh vacuum chamber with a base pressure of better than $1x10^{-8}$ Torr.

Electrochemical characterization

Cyclic voltammetry (CV) was performed on the Ni sample using a Bio-Logic SP-150 potentiostat, with the sample as working electrode and connected to the common ground. Fig. 5c shows a cyclic voltammogram (-0.1 $V_{Ag/AgCl}$ to +0.65 $V_{Ag/AgCl}$) for the thin Ni layer immersed in a 0.1 M KOH solution, with characteristic oxidation and reduction peaks at +0.5 $V_{Ag/AgCl}$ and +0.4 $V_{Ag/AgCl}$, respectively, in good agreement with literature data.[38,39] The stability of the sample inside the solution was tested in repeated cyclic voltammograms over the course of several hours, during which the voltammograms showed little change. The measurements on the thin Ni film deposited onto the multilayer mirror were also compared to those on a bulk polycrystalline Ni foil and showed very good agreement.

APXPS and Standing wave measurements

The basic principle of SWAPPS is shown in Figure 4. Focused X-rays are incident on the sample at the first-order Bragg angle of the multilayer mirror, defined from $\lambda_x = 2d_{ML}sin\theta_{inc}$, where λ_x is the X-ray wavelength, d_{ML} is the multilayer period, and θ_{inc} is the X-ray incidence angle, in the present case 3.5° for 3.1 keV X-rays and a multilayer periodicity of 3.4 nm. This leads to the formation of a standing wave above the mirror with a wavelength λ_{sw} close to the mirror periodicity[40,41]. The SW extends above the mirror (*i.e.*, through the deposited Ni film and the adsorbed solution layer) in the volume where the incident and reflected X-rays overlap, and is scanned vertically by changing the incidence angle (rocking curve), thus selectively probing the interface, the bulk solid or bulk liquid (cf. Fig. 4). Core photoelectron peak intensities from different chemical states in the sample are then monitored as a function if incidence angle, with the resultant variations being characteristic of the depth distribution of a given species. Beyond simple Bragg reflection from the mirror, interference due to X-rays reflected from the top of the sample and from other interfaces in the sample (e.g. the mirror surface) can lead to additional fine structure in the rocking curves that are often referred to as Kiessig fringes[40,41], with these also containing structural information. These in general are described by $m\lambda_x = 2Dsin\theta_{inc}$, where m is the usually unknown order = 1,2,3,…. and D is the distance between the surface of the sample

and the reflecting interface. For the commonly very large m in experiment, the separation between these fringes can be used to estimate the distance involved from $D(nm) = 0.62/[h\nu(eV)\Delta\theta(rad)]$, where $h\nu$ is the photon energy. For more detailed discussions of the technique see Refs. 32, 35, 36, 40, 41. The combination of the standing wave approach and the intrinsic surface sensitivity of XPS is then used for the determination of the vertical positions and widths of all interfaces present in the system.

The measurements were performed at beamline 6.0.1 at the Advanced Light Source in Berkeley, CA, using a Phoibos NAP 150 electron energy analyzer (Specs Surface Nano Analysis GmbH, Berlin). The incident X-rays had a photon energy of 3100 eV. The incident photon flux at this energy is ~10^{12} photons/s. The measurement geometry is shown in Fig. 5a. The sample-aperture distance is estimated to be 0.2 mm. The incident X-ray beam spot is about 0.1 mm, but is horizontally enlarged by about 16 times due to the shallow incidence angle on the sample of ~3.5°. Ni 2p, O 1s, and C 1s spectra were collected under all experimental conditions. Valence band spectra taken under dry conditions were used to calibrate the binding energy scale. The sample was connected to the common ground in all experiments. Due to the strong attenuation of the photoelectron signal by the water gas phase, at a pressure of ca. 17 Torr, acquisition times of up to 5 minutes for a single energy region were necessary, in particular for the Ni 2p and 3p core levels, where attenuation due to adsorbed water or the KOH solution led to additional attenuation of the signal. The Ni 3p and O 1s spectra for the rocking curves were taken in the "snapshot mode" using a 2D delayline detector. Pass energies of 200 eV and 150 eV were used for the Ni 3p and O 1s regions, respectively, giving binding energy windows of 19.9 eV and 14.9 eV, sufficient for the capture of all spectral components. The complete rocking curve measurement took approximately 5 hours. An angle step size of 0.02° was used in the experiments. The precision of the manipulator's rotation was measured with a Möller-Wedel ELCOMAT 3000 autocollimator, and shown to be reliable at least down to a step size of 0.005°.

Data analysis

The X-ray optical and photoemission simulations were performed using the Yang X-Ray Optics (YXRO) software,[40,41] which simulated the depth distribution of the electric field strength as a function of beam incidence angle and also the photoemission rocking curves for different layers and elements. As a qualitative indicator of the anticipated sensitivity to vertical position in such rocking curve measurements, Figure 6 shows a set of such curves as a "delta layer" is moved in 0.1 nm steps vertically through a hypothetical liquid layer on top of a multilayer of our configuration. These results indicate that, with the 3100 eV photon energy and multilayer mirror

we have used, peaks separated by 0.02° originate from regions of the sample that are 0.7 nm apart. A key parameter in these calculations is the inelastic mean free paths for photoelectrons of the relevant core levels in liquid water; these are taken from Emfietzoglou and Nikjoo[26], and can also be found in Table 1 (see below). The values for the IMFP in liquid water agree well with theoretical predictions by Tanuma, Powell, and Penn.[42]

Results and discussion

In the following we will describe proof-of-principle measurements of combining the meniscus method and SWAPPS measurements to study the interface of a 0.1 M KOH solution with polycrystalline Ni. We will first show results of static measurements before discussing the findings from rocking curve SWAPPS experiments.

Before the SWAPPS measurements the state of the Ni thin film was investigated under three different conditions: As prepared ("dry"), in the presence of high relative humidity ("humid"), and after preparation of a thin KOH film using the meniscus method ("immersed"). Under dry conditions (background pressure $1x10^{-2}$ Torr), the sample was already covered by an oxide/hydroxide layer, which was most likely formed due to exposure to ambient conditions before moving the sample into the chamber. Ni $2p_{3/2}$, O 1s and C 1s spectra are shown in Figure 7. The literature value for the O 1s peak of the oxide is 529-530 eV. [43] We thus suggest that the oxide peak appears as a shoulder to the broad peak centered around 531.5-532.0 eV, and that this broad peak is mainly due to Ni hydroxides (BE ~531 eV) and oxygen containing carbonaceous contamination. The Ni $2p_{3/2}$ spectrum shows that not all of the Ni film is oxidized or hydroxylated, and also that the oxide/hydroxide layer is thin compared to the probing depth in these measurements since the Ni 2p spectrum shows mainly a sharp metallic Ni peak at BE ~853 eV. The calculation of the oxide/hydroxide layer thickness for this dry state, using the standing-wave technique under UHV, shows a thickness of 1.8 nm. The carbon overlayer thickness is 0.8 nm from the same analysis. The C 1s signal consists of at least two peaks, which we assign to hydrophilic (oxygenated, high BE) and hydrophobic (non-oxygenated, low BE) carbon.

After the dry measurements the Ni sample was investigated under humid conditions at a water vapor pressure of 17 Torr, which corresponds to ~85 % RH at a sample temperature of 22 °C. The water vapor was supplied from degassed pure water; no KOH solution was present in the chamber in the experiments under humid conditions. There is a significant decrease in the intensity of all XPS signals due to scattering of electrons by water vapor. In addition, the Ni 2p, Ni 3p (not shown) and O 1s signals from Ni metal and Ni oxide/hydroxide are attenuated by the liquid water layer which is present at this high RH. A quantitative analysis of the decrease of the

C 1s signal is consistent with a model where, under humid conditions, a similar amount of carbon as in the "dry" sample is present, with attenuation only by the water vapor. This indicates that most of the carbon contamination is located at the liquid/water vapor interface. Sources for the carbon contamination under humid conditions are the original contamination on the "dry" sample, but also additional contamination from the background vapor due to the limited pumping during the experiments at high humidity. There is no detectable change in the main Ni $2p_{3/2}$ peak position, which indicates that Ni is still mostly in the metallic state. The gas phase water peak is the most intense peak in the O 1s spectrum. The liquid water layer that is formed at high RH has an O 1s peak at 533-534 eV, which effectively broadens the Ni oxide/hydroxide signal centered around 532 eV towards higher binding energies. Thus, the broad O 1s signal around 532 eV is a combination of liquid water, oxide and hydroxides of Ni, and O containing carbonaceous contamination.

The thickness of the liquid water layer can be estimated from the Ni 2p and Ni 3p signals before and after the introduction of the vapor into the chamber using

$$\frac{I_{Ni}}{I_{0,Ni}} = \exp\left(-\frac{d_w^L}{\lambda_w^L\ cos\theta}\right)\exp\left(-\frac{d_w^G}{\lambda_w^G}\right), \qquad (1)$$

with $I_{0,Ni}$ as the Ni signal intensity for the "dry" sample, I_{Ni} the Ni signal intensity for the "humid" or the "immersed" sample, λ_w^L the inelastic mean free path of electron in liquid water, λ_w^G the inelastic mean free path of electron in gaseous water, θ the angle between the surface normal and the analyzer axis (45°), d_w^L the thickness of the liquid water layer, and d_w^G the effective thickness of the water vapor that the electrons traverse before reaching low vacuum conditions in the first differential pumping stage (*i.e.*, approximately the sample aperture distance of ~300 μm). The equation can be simplified combining the two terms on the right-hand side, under assumption of a hypothetical liquid layer (without the vapor) which gives the same I/I_0 value.

$$\frac{I_{Ni}}{I_{0,Ni}} = \exp\left(-\frac{d_w^{Leq}}{\lambda_w^L\ cos\theta}\right) \qquad (2)$$

with

$$d_w^{Leq} = d_w^L + d_w^G\frac{\lambda_w^L}{\lambda_w^G}\cos\theta\ . \qquad (3)$$

The ratio of the inelastic mean free-paths in water vapor compared to liquid water is approximately the inverse of the densities of these media, such that:

$$\frac{\lambda_w^L}{\lambda_w^G} \approx \frac{\rho_w^G(17\text{ Torr, }20\text{ °C})}{\rho_w^L} = \frac{17\text{ g/m}^3}{10^6\text{ g/m}^3} = 1.7\times10^{-5}\ . \qquad (4)$$

From combining Eqs. 3 and 4, and considering that $cos\theta = cos45° = 0.707$, it follows that

$$d_w^{Leq} = d_w^L + d_w^G \frac{\lambda_w^L}{\lambda_w^G} \cos\theta = d_w^L + (200\ \mu m)(1.7 \times 10^{-5})(0.707), \quad (5)$$

which yields $d_w^{Leq} = d_w^L + 2.4$ nm. Based on this analysis, the thickness of the liquid water layer is estimated to be 11-13 nm. The parameters and data that are used in the calculation are summarized in Table 1.

Table 1. Data and parameters used for the calculation of liquid water layer thickness under "humid" and "immersed" conditions.

			Dry	Humid	Immersed	Humid	Immersed
Core level	Electron kinetic energy (eV)	IMFP (nm)	Intensity (CPS eV)			d_w^L (nm)	
Ni 2p	~2240	7.5	48000	2560	1100	13	18
Ni 3p	~3030	9.0	11400	1510	300	11	21
C 1s	~2820	8.5	2300	860	2380	-	-

After the sample was immersed in 0.1 M KOH solution, several CV cycles were run between +0.65 and -0.9 $V_{Ag/AgCl}$ before stopping at +0.6 $V_{Ag/AgCl}$ during the anodic sweep. Data were acquired at a constant potential of +0.6 $V_{Ag/AgCl}$ for the spectra shown in Fig 7. From Pourbaix diagrams[44] of Ni, as well as from assignments of the CV features[38], we expect the presence of hydroxides and oxyhydroxides at the interface under the pH and bias in our experiments. This is borne out by the Ni 2p spectrum, where the main peak BE has shifted to 856 eV, close to the literature value for oxide/hydroxide/oxyhydroxide. The O 1s spectrum shows a much stronger contribution from liquid water, as compared to the "humid" sample. The O 1s gas phase peak shifts to lower BE (higher KE) as expected from a negative potential applied to the solution; the gas phase peak shift confirms that the part of the liquid film under investigation is connected to the bulk solution reservoir. The water vapor peak shifts by ~0.4 eV, compared to the expected value of 0.6 eV for a full shift due to the applied bias. This can explained by the fact that gas phase peaks shifts less than surface peaks due to the pinning of the vacuum level of the gas phase to that of the sample and surrounding surfaces.[15,17] The C 1s spectra show the existence of at least 2 peaks (hydrophilic/hydrophobic), however, their intensity is now higher than the C 1s intensity for the "dry sample". This might be an indication that, during the retraction of the sample from the solution, a Langmuir-Blodgett-type film deposition of hydrocarbons took place due to hydrophobic molecules floating on the surface of the solution in the cell (e.g., from trace contamination of the KOH solution or the water that was used for dilution). Another contribution to the extra carbon is probably residual CO_2 that is strongly absorbed into the liquid to form

HCO_3^-. The K 2p signal which is expected at ~ 293 eV is not clearly visible. For a 0.1 M KOH solution, the K/H_2O ratio is ~1/550 and thus too low to observe K in the bulk of the solution using XPS. Using the previously explained analysis method, the thickness of the liquid water layer under immersed conditions is estimated to be 18-21 nm, *i.e.* ~50-100% thicker than the water layer under "humid" conditions.

We now proceed to discussing the results of the standing wave measurements using SWAPPS, where we compare measurements of the dry sample with those of the sample under immersed conditions. An initial experimental characterization of the dry sample using standing-wave photoemission was performed under UHV conditions at beamline 9.3.1 of the Advanced Light Source. The structure and composition of the sample was revealed through measuring Ni $2p_{3/2}$ and O 1s rocking curves and by an iterative simulation of the rocking curves, followed by a comparison with their experimental counterparts (Figure 8, left panel) using the methods described in the experimental section. The measured rocking curves for the two core-level spectra (Ni $2p_{3/2}$, O 1s) are thus representative of the two primary layers: metallic Ni, and the oxidized Ni surface. All curves are normalized to their maxima. The metallic Ni layer was found to be 6.8 nm thick, capped by 1.8 nm of oxidized nickel, most likely in the form of NiO. The roughness of the interface between Ni and NiO and the top of the NiO layer is 1.0 nm, which is somewhat larger than the ca. 0.5 nm roughness measured by AFM for the Ni film just after growth. The carbon contamination layer at the surface is 0.8 nm thick, and we do not show any rocking curves from this contaminant element. This experimentally-determined model of the dry sample was used as a starting point for the analysis of the sample under immersed conditions.

In the immersed case, spectra of two regions were again collected: Ni 3p and O 1s. Ni 3p and O 1s spectra were fitted with 1 doublet and 3 peaks, respectively. The rocking curves in the middle panel of Fig. 8 show the peak intensities normalized to their mean value, as a function of incidence angle of the X-ray beam and the results of the simulation for the optimized sample structure as a solid line. The initial analysis of the nickel (from Ni 3p), which we assume is present in form of hydroxide/oxyhydroxide, as discussed previously for the static data, and the solution layer thicknesses (from O 1s) revealed that both of those layers are much thicker than a standing wave period (~ 3.4 nm) and therefore there are several nodes and antinodes in different depths buried within those layers (see the electric field plot - Figure 8, right panel). The examination of such thick layers using standing wave photoemission, especially with harder X-rays (larger IMFPs), has an additional challenge. At these high kinetic energies (> 2 keV) photoelectrons carry information from a larger depth and the intensity modulation at the Bragg angle is attenuated due to the signal integration along the axis perpendicular to the sample

surface. This is the case in the present experiment and evidenced by the observation that the standing wave features in the rocking curves for the immersed sample are much broader and show smaller amplitudes than those from the thin layers of the dry sample.

Other relatively strong features adjacent to the Bragg peak and with a period of ~ 0.02° are observed in the rocking curves measured on the immersed sample. These are no doubt due to some kind of Kiessig interference, and we can estimate the *D* value involved from the prior equation to be about 40-60 nm, which is roughly the distance from the surface of the liquid film to the top of the multilayer mirror. In order to fully identify the origin of these oscillations, one has to examine the angular and depth dependence of the electric field strength (Figure 8, right). The period of the standing wave is decreasing as the incidence angle of the X-rays is increasing, a trend expected from the two interfering waves involved. With increasing distance from the surface of the mirror, the difference of the standing wave phase for angles below and above the Bragg angle increases and the maxima are enhancing the photoemission signal from different depth at the different angles. These features, which in their period along the depth axis deviate slightly from the period of the mirror, are responsible for the observed oscillations in the O 1s rocking curves. They have proven to be especially helpful in determining the exact position of, as well as interdiffusion between, the different interfaces for thicker samples, as these features have different periods in depth compared to the main Bragg peaks generated by the mirror and therefore the standing-wave analysis can overcome the uncertainty in depth position caused by the presence of multiple nodes and antinodes of the standing-wave within one layer of the sample.

Using the iterative fitting of the X-ray optical and photoemission simulations to the experimental data, the thickness of the hydroxide/oxyhydroxide layer for the immersed sample was found to be 27 nm, with a water layer thickness of 20 nm. The surface of the wet layer is perfectly sharp within our depth resolution (<1 nm), while the interface between the hydroxide/oxyhydroxide layer and the KOH solution is exhibiting a roughness of 1 nm. The thickness of the hydroxide/oxyhydroxide layer also agrees well with the expected value for the expansion of the originally ~ 8 nm of metallic Ni transformed into a stoichiometric hydroxide by approximately a factor of 3.4, *i.e.* to ~27 nm. Under the given pH and bias conditions, no significant dissolution of Ni is expected. The standing wave analysis concurs with this expectation, as all of the Ni atoms are located in the solid layer according to the proposed model. A schematic of the proposed structural models for the Ni sample under dry and immersed conditions is shown in Figure 9. The general model takes into consideration the expansion of the dry nickel film into oxidized/hydroxylated nickel, as well as the quantitative analysis of the Ni signal attenuation for the immersed sample. The standing wave analysis enabled refinement of

these rough estimates by determining the positions of the interfaces and surfaces with high precision (within one period of the standing wave) and also provides unique information on the interfacial and surface roughness.

Conclusions

The preceding data and discussion show that SWAPPS, combined with hard X-rays and with the preparation of thin solution layers using the meniscus method, is an exciting new approach to characterize all components of the liquid/solid interface, from bulk species in the liquid and solid to species located at the interface under potential control. In this paper, we determined the complete oxidation/hydroxylation of an 8 nm thick Ni film in the presence of a 20 nm thick 0.1 M KOH solution at a bias of +0.6 $V_{Ag/AgCl}$. This measurement would not have been possible in a conventional XPS experiment without the use of the standing wave method, which provides an intrinsic ruler in the direction perpendicular to the interface and extends the probing depth and the depth resolution in XPS. We anticipate that the resolution of the method can be further increased by using longer periods of the standing wave and by measuring more of the Kiessig fringes adjacent to the Bragg peak. The range of applications in corrosion science thus seems to be very large.

Acknowledgements

This work was supported by Laboratory Directed Research and Development projects through Lawrence Berkeley National Laboratory. The ALS and its beamlines 6.0.1 and 9.3.1 are supported by the Director, Office of Science, Office of Basic Energy Sciences of the US Department of Energy at the Lawrence Berkeley National Laboratory under Contract No. DE-AC02-05CH11231. HB, OK, AS, IZ, MH, and CR acknowledge support by the Director, Office of Science, Office of Basic Energy Sciences, and by the Division of Chemical Sciences, Geosciences, and Biosciences of the US Department of Energy at the Lawrence Berkeley National Laboratory under Contract No. DE-AC02-05CH11231. SN and CF also acknowledge support from the DOE Division of Materials Sciences, also under Contract DE-AC02-05CH11231 and ARO-MURI grant W911-NF-09-1-0398. Kai Liu, Peter K. Greene and Edward C. Burks (UC Davis) are acknowledged for the preparation of the Ni sample and AFM characterization of the as prepared samples. MH acknowledges support from the Deutscher Akademischer Austauschdienst (DAAD). M.L. Ng gratefully acknowledges the financial support from Wenner-Gren Foundations in Stockholm, Sweden. CF was also supported during this work by the French LabEx PALM, APTCOM Project, no. ANR-10-LABX-0039.

References

1 E. McCafferty, *Introduction to Corrosion Science*, Springer, New York, 2009.

2 S. J. Peters and G. E. Ewing, *J. Phys. Chem. B*, 1997, **101**, 10880.

3 V. Sadtchenko, G.E. Ewing, D.R. Nutt and A.J. Stone, *Langmuir*, 2002, **18**, 4632.

4 Y.R. Shen, *Nature*, 1989, **337**, 519.

5 G. Rupprechter, *MRS Bulletin*, 2007, **34**, 1031.

6 J. Forsberg, L.C. Duda, A. Olsson, T. Schmitt, J. Andersson, J. Nordgren, J. Hedberg, C. Leygraf, C. Asstrup, D. Wallinder, and J.-H. Guo, *Rev. Sci. Instrum.*, 2007, **78**, 083110.

7 J.-J. Velasco-Velez, C.H. Wu, T.A. Pascal, L.F. Wan, J. Guo, D. Prendergast and M. Salmeron, *Science*, 2014, **346**, 831.

8 S. Ferrer, M.D. Ackermann and E. Lundgren, *MRS Bulletin*, 2007, **32**, 1010.

9 G. Binnig, C.F. Quate and Ch. Geber, *Phys. Rev. Lett.*, 1986, **56**, 930.

10 J. Hu, X.-d. Xiao, D.F. Ogletree and M. Salmeron, *Science*, 1995, **268**, 267.

11 B.L.M. Hendriksen and J.W.M. Frenken, *Phys. Rev. Lett.*, 2002, **89**, 046101.

12 M.J. Williamson, R.M. Tromp, P.M. Vereecken, R. Hull, and F.M. Ross, *Nat. Mater.*, 2003, **2**, 532.

13 S. Thiberge, A. Nechushtan, D. Sprinzak, O. Gileadi, V. Behar, O. Zik, Y. Chowers, S. Michaeli, J. Schlessinger, and E. Moses, *E. Proc. Natl. Acad. Sci. U. S. A.*, 2004, **101**, 3346.

14 F. Zaera, *Chem. Rev.*, 2012, **112**, 2920.

15 E.J. Crumlin, H. Bluhm and Z. Liu, *J. Electr. Spectrosc. Rel Phenom.*, 2013, **190**, 84.

16 D. E. Starr, Z. Liu, M. Hävecker, A. Knop-Gericke and H. Bluhm, *Chem. Soc. Rev.*, 2013, **42**, 5833.

17 H. Bluhm, *J. Electron Spectrosc. Relat. Phenom.*, 2010, **177**, 71.

18 M. Salmeron and R. Schlögl, *Surf. Sci. Rep.*, 2008, **63**, 169.

19 S. Yamamoto, K. Andersson, H. Bluhm, G. Ketteler, D.E. Starr, Th. Schiros, H. Ogasawara, L.G.M. Pettersson, M. Salmeron and A. Nilsson, *J. Phys. Chem. C*, 2007, **111**, 7848.

20 K. Andersson, G. Ketteler, H. Bluhm, S. Yamamoto, H. Ogasawara, L.G.M. Pettersson, M. Salmeron and A. Nilsson, *J. Am. Chem. Soc.*, 2008, **130**, 2793.

21 A. Verdaguer, G.M. Sacha, H. Bluhm and M. Salmeron, *Chem. Rev.*, 2006, **106**, 1478.

22 G.E. Ewing, *Chem. Rev.*, 2006, **106**, 1511.

23 D.M. Kolb, D.L. Rath, R. Wille and W.N. Hansen, *Ber. Bunsen-Ges. Phys. Chem.*, 1983, **87**, 1108.

24 E.R. Kötz, H. Neff and K.J. Müller, *Electroanal. Chem. Interfacial Electrochem.*, 1986, **215**, 331.

25 W. Zhou and D.M. Kolb, *Surf. Sci.*, 2004, **573**, 176.

26 D. Emfietzoglou and H. Nikjoo, *Radiation Research*, 2007, **167**, 110.

27 S. Axnanda, E.J. Crumlin, B. Mao, S. Rani, R. Chang, W. Stolte, P.G. Karlsson, M.O.M. Edwards, M. Lundqvist, R. Moberg, P.N. Ross, Z. Hussain and Z. Liu, submitted.

28 M. Faubel, B. Steiner and J.P. Toennies, *J. Chem. Phys.*, 1997, **106**, 9013.

29 M.A. Brown, N. Duyckaerts, A. Beloqui Redondo, I. Jordan, F. Nolting, A. Kleibert, M. Ammann, H.J. Wörner, J.A. van Bokhoven and Z. Abbas, *Langmuir*, 2013, **29**, 5023.

30 A. Kolmakov, D.A. Dikin, L.J. Cote, J. Huang, M.K. Abyaneh, M. Amati, L. Gregoratti, S. Günther, and M. Kiskinova, *Nat. Nanotechn.*, 2011, **6**, 651.

31 K. Arima, P. Jiang, X. Deng, H. Bluhm and M. Salmeron, *J. Phys. Chem. C,* 2010, **114**, 14900.

32 S. Nemšák, A. Shavorskiy, O. Karslioglu, I. Zegkinoglou, P.K. Greene, E.C. Burks, K. Liu, A. Rattanachata, C.S. Conlon, A. Keqi, F. Salmassi, E.M. Gullikson, S.-H. Yang, H. Bluhm and C.S. Fadley, *Nat. Comm.*, 2014, **5**:5441, doi: 10.1038/ncomms6441.

33 J. O'M. Bockris and B.D. Cahan, *J. Phys. Chem*., 1969, **50**, 1307.

34 P.-G. de Gennes, F. Brochard-Wyart, D. Quéré, *Capillarity and Wetting Phenomena*, Springer, New York, 2004.

35 C.S. Fadley, *J. Electron Spectrosc. Relat. Phenom.*, 2013, **190**, 165.

36 A.X. Gray, *J. Electron Spectrosc. Relat. Phenom.*, 2014, **195**, 399.

37 D. Weingarth, A. Foelske-Schmitz, A. Wokaun and R. Kötz, *Electrochem. Commun.*, 2011, **13**, 619.

38 K. Wang, G.S. Chottiner and D.A. Scherson, *J. Phys. Chem.*, 1993, **97**, 10108

39 P.F. Luo, T. Kuwana, D.K. Paul and P.M.A. Sherwood, *Anal. Chem.*, 1996, **68**, 3330.

40 S.-H. Yang, A.X. Gray, A.M. Kaiser, B.S. Mun, B.C. Sell, J.B. Kortright and C.S. Fadley, *J. Appl. Phys.*, 2013, **113**, 073513.

41 S.-H. Yang, X-Ray Optics (YXRO) program for simulating standing-wave photoemission above multilayers, https://sites.google.com/a/lbl.gov/yxro/home (2011).

42 S. Tanuma, C. J. Powell and D. R. Penn, *Surf. Interf. Anal.*, 1993, **21**, 165

43 M.C. Biesinger, B.P. Payne, L.W.M. Lau, A. Gerson and R.St.C. Smart, *Surf. Interface Anal.*, 2009, **41**, 324.

44 B. Beverskog and I. Puigdomenech, *Corros. Sci.*, 1997, **39**, 969.

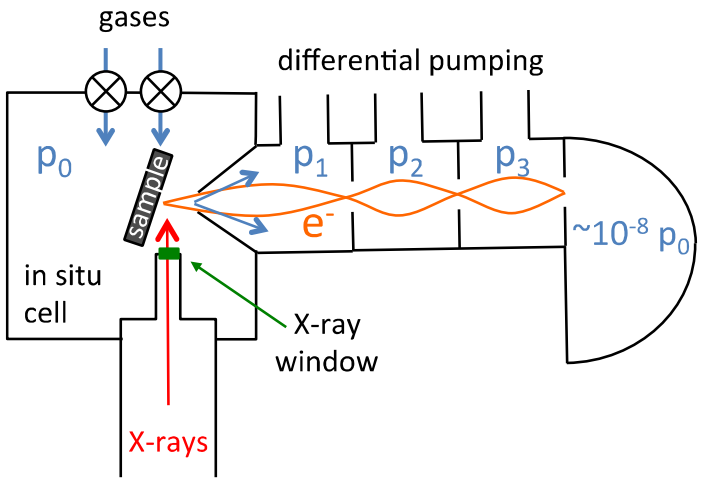

Figure 1

Principal layout of a typical APXPS experiment. The sample is located inside the in situ cell, which is backfilled with a gas or gas mixture to a pressure p_0. X-rays from a laboratory source (X-ray anode) or synchrotron beamline are admitted to the in situ cell through an X-ray transparent window, most often silicon nitride with a thickness of ~100 nm and an active area of ~1 mm^2. The sample is placed in close proximity of the entrance aperture of the differentially pumped lens system of a hemispherical electron analyzer. The typical aperture size is ~0.1 mm^2, and the typical sample-aperture distance about 1 mm. Electrons and gas molecules escape through the entrance aperture into the first differential pumping stage, which is typically at a pressure of $p_1 < 10^{-3}$ p_0, *i.e.* scattering of electrons by gas molecules in the first differential pumping stage is greatly reduced. Many APXPS systems feature several differential pumping stages, which successively decrease the pressure by several orders of magnitude. Electrostatic lenses in the differential pumping stages focus the electrons onto the apertures that separate the stages, thus maintaining a similar solid angle of electron detection as in a vacuum-based XPS instrument.

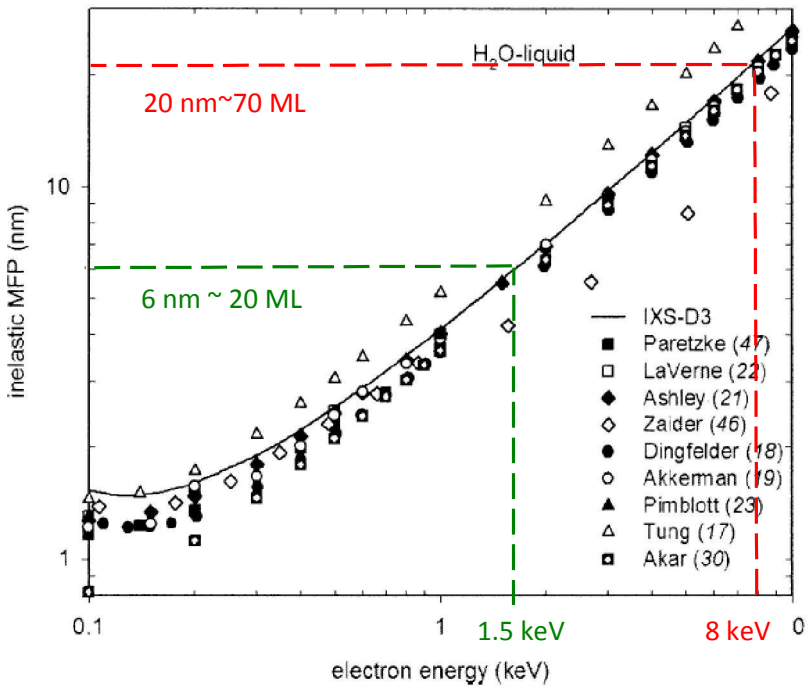

Figure 2

Electron inelastic mean free path in liquid water as a function of electron kinetic energy. For the excitation energy of an Al K-alpha lab source (1486.7 eV) the maximum IMPF is about 6 nm, which corresponds to a water film thickness of about 20 monolayers. At higher excitation energies, e.g. 8 keV, which is a realistic value for high KE APXPS instruments, the mean free path increases to ~ 20 nm, or ~ 70 monolayers of water. The drawback of higher photon energies is the lower photoemission cross section and thus the decrease in the photoemission intensity. Adapted and reproduced with permission from Ref. [26].

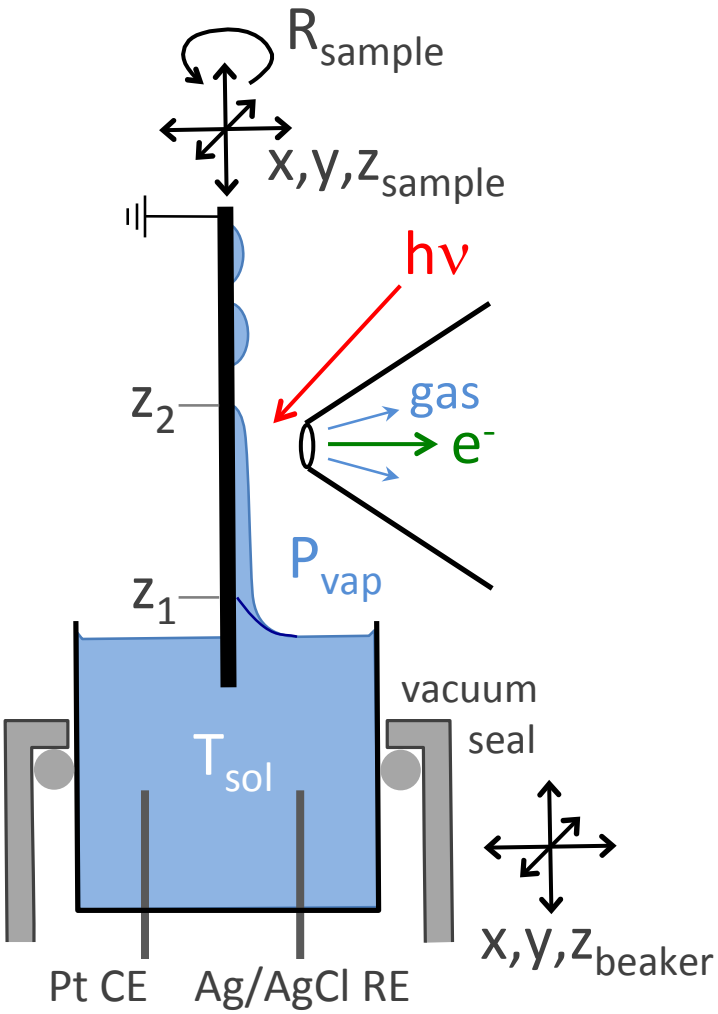

Figure 3

Schematic of the meniscus method for the preparation of thin liquid films. For hydrophilic surfaces the meniscus will extend to a height z_1 (for neat water a few mm) above the bulk solution surface (for simplicity the formation of the liquid film is shown for only one side of the sample). Under favorable conditions and in the presence of water vapor pressures close to saturation a thin liquid film can be stabilized over the whole range that the sample was originally dipped into the solution (z_2). This part of the film is in electrical contact with the bulk solution. The front aperture of the differentially pumped lens system of the APXPS system is also shown. For full electrochemical control, a counter and reference electrode are placed into the solution, while the sample (working electrode) is held on ground potential, in case of a metal with its Fermi level aligned to that of the photoelectron spectrometer.

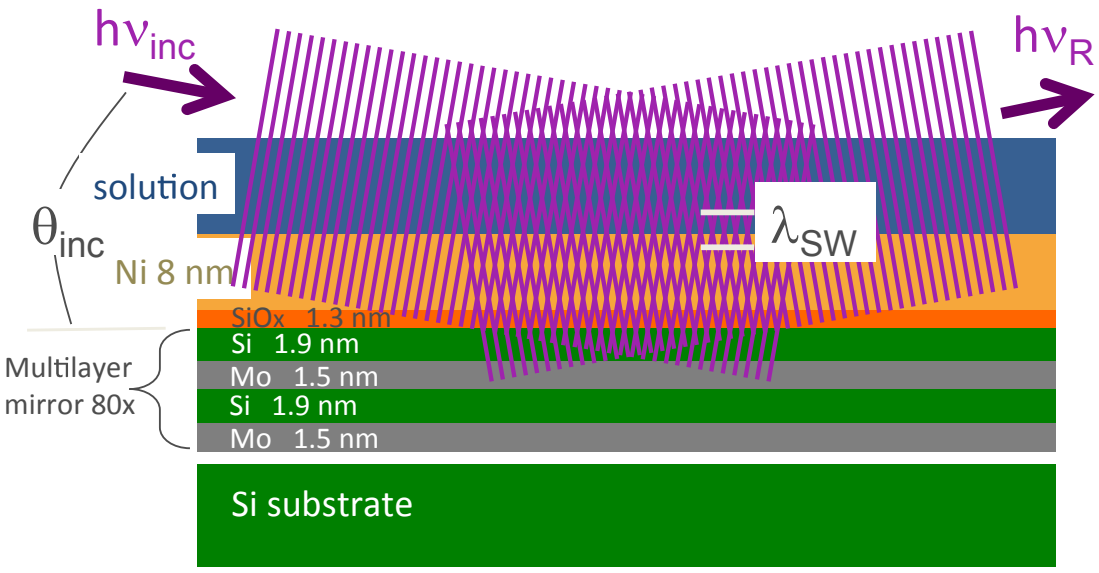

Figure 4

Principal layout of a SWAPPS experiment, with the dimensions of the multilayer and sample indicated as used in the present experiments. The Si/Mo multilayer mirror with a periodicity of 3.4 nm is grown onto a Si substrate. Incident photons ($h\nu$ = 3.1 keV) are reflected off the multilayer mirror under the first order Bragg angle ($\theta_{inc} \sim 3.5°$) and interfere with the reflected X-rays, leading to the formation of a standing wave with a periodicity close to that of the multilayer mirror in the direction perpendicular to the surface. When the incidence angle of the X-rays is changed around the first order Bragg condition (rocking curve), both the amplitude and the phase of the standing wave change. The Ni sample is grown on top of the SiO_2 cap layer of the multilayer mirror. The phase change during a rocking curve shifts the standing wave by a distance of half of its wavelength and thus allows to vary the amplitude of the standing wave across the metal/solution interface.

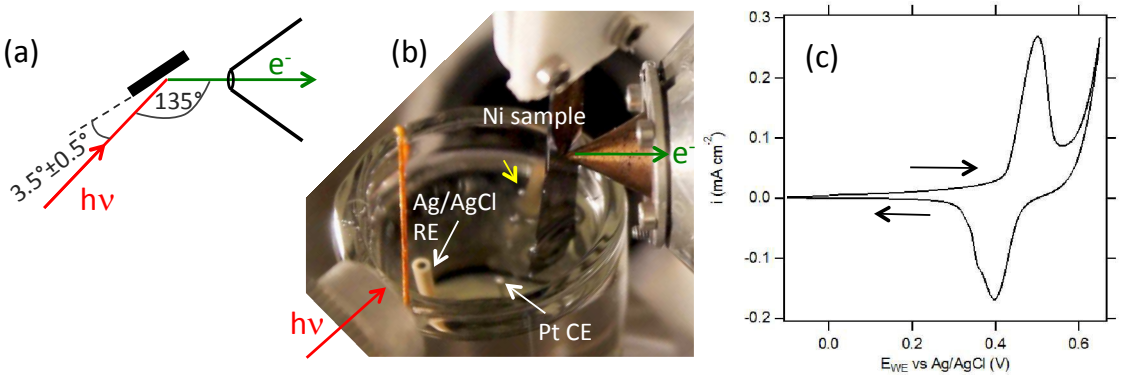

Figure 5

(a) Top view of the measurement geometry in the SWAPPS experiments. **(b)** Photograph of the sample inside the measurement chamber, dipped into a 0.1 M KOH solution at +0.6 $V_{Ag/AgCl}$. The yellow arrow indicates a bubble that is formed in the solution. **(c)** Cyclic voltammogram of a nickel film on top of a multilayer structure in 0.1 M KOH taken inside the measurement chamber in the configuration shown in (b). The scan rate was 20 mV/s.

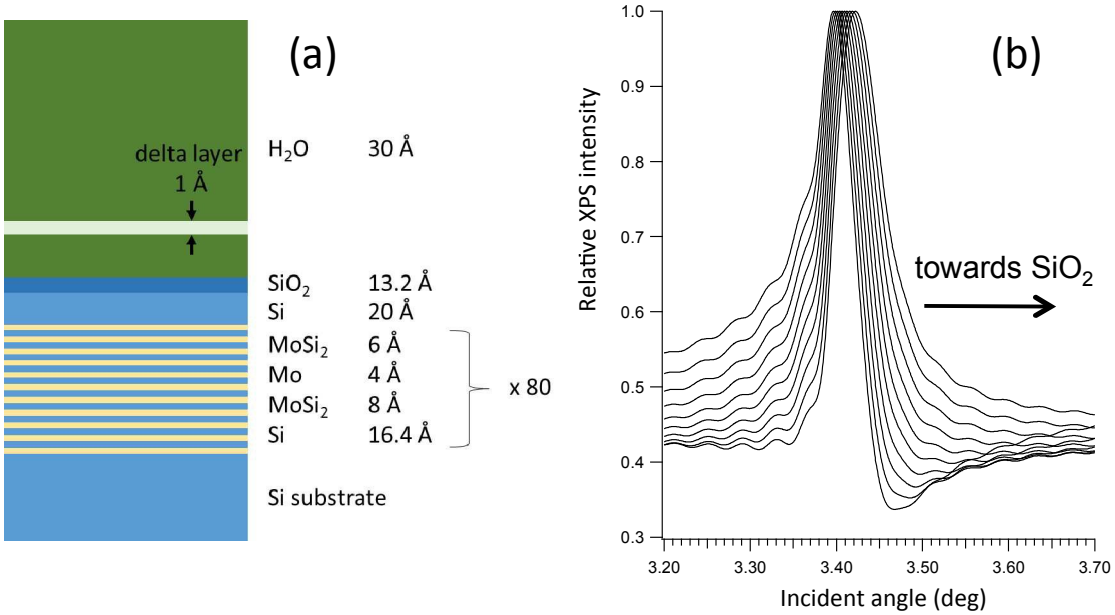

Figure 6

Determination of the sensitivity in the present SWAPPS rocking curves to depth, using an incident photon energy of 3100 eV. **(a)** Layout of the model system used in the calculations. A water "delta layer" of 0.1 nm thickness is scanned through a 1 nm thick water layer on top of a SiO_2 cap layer on the multilayer mirror. **(b)** Calculated O 1s rocking curves, in steps of 0.1 nm changes of the height of the "delta layer" above the SiO_2/water interface. Both the peak position as well as the shape of the curves are changing as a function of the distance of the "delta layer" from the SiO_2 interface. A shift in the peak position of the rocking curve by 0.02 deg corresponds to a distance of 0.7 nm.

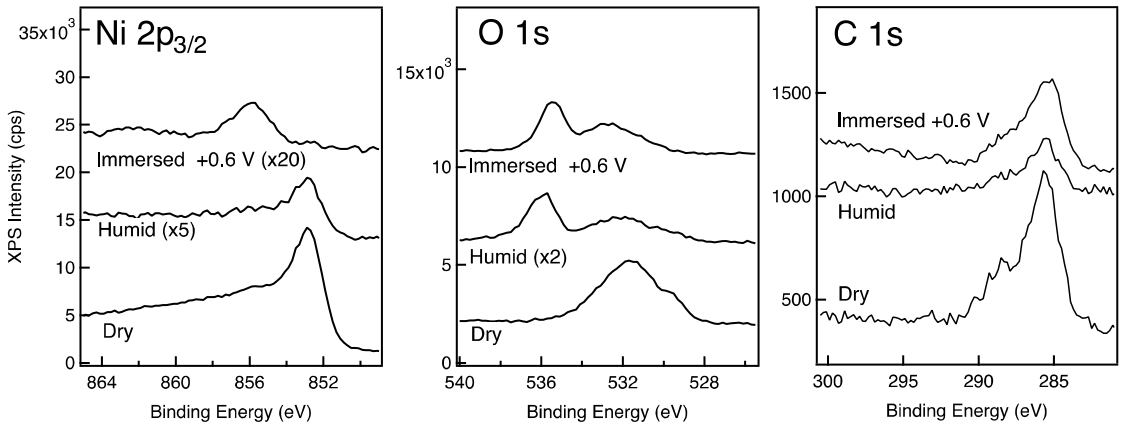

Figure 7

Ni $2p_{3/2}$, O 1s and C 1s APXPS spectra of the Ni sample deposited onto the multilayer mirror taken under three different conditions: As is, in low vacuum (10^{-2} Torr, "Dry"); in the presence of 17 Torr water vapor ("humid"); and after forming a thin KOH solution film using the meniscus method, at a potential of +0.6 $V_{Ag/AgCl}$ ("immersed"). All measurements were done at room temperature.

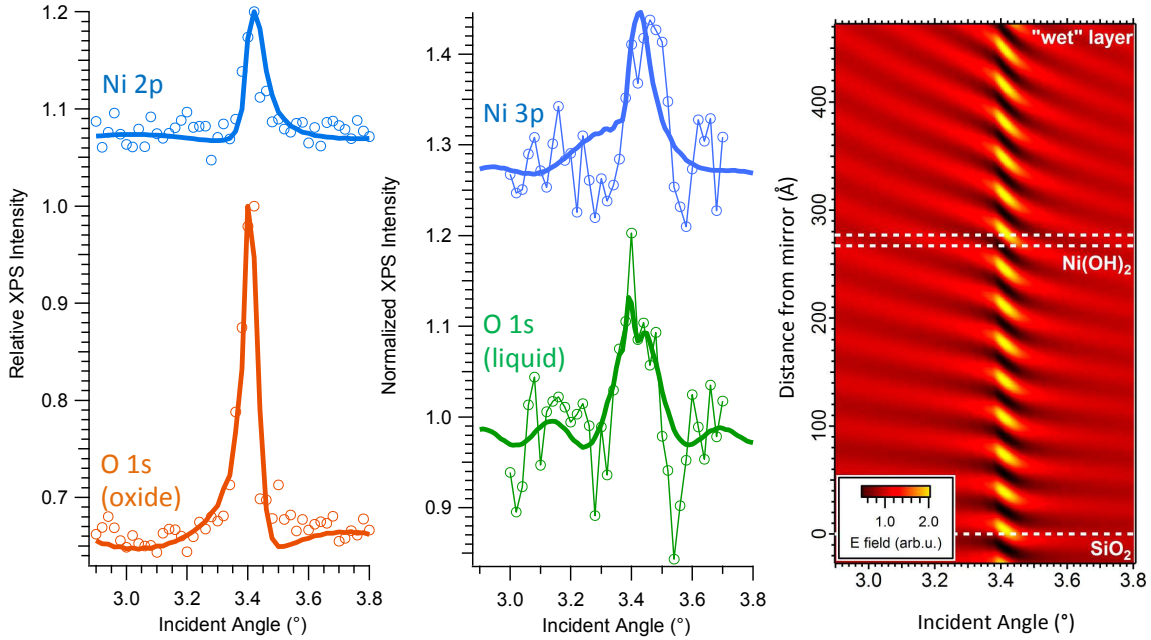

Figure 8

SWAPPS rocking curves (dots) and iterative fits (solid lines) taken under different conditions: **Left panel**: Ni $2p_{3/2}$ and O 1s (oxide component) for the as-prepared sample, in ultra-high vacuum; **Middle panel**: Ni 3p and O 1s (liquid component) for a sample with a thin KOH solution film prepared using the meniscus method, at a potential of +0.6 $V_{Ag/AgCl}$; **Right panel**: Simulated electric field strength as a function of beam incidence angle and depth for the immersed sample (rocking curves in the middle panel). White dashed lines show the boundaries between the "wet" layer and $Ni(OH)_2$ and between $Ni(OH)_2$ and the multilayer mirror.

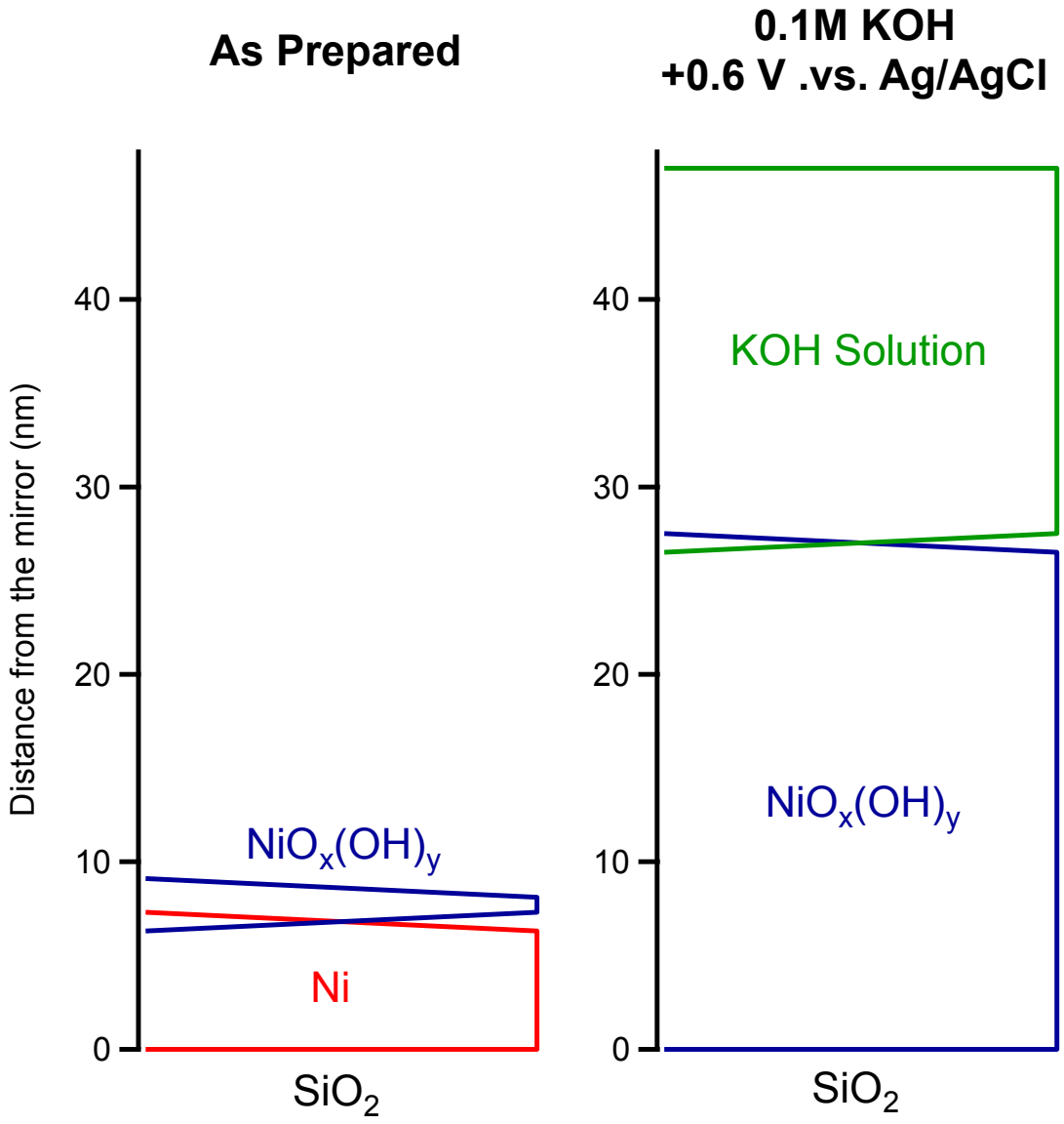

Figure 9

Model based on the detailed analysis of the rocking curves in Fig. 8, showing the relative concentration profiles of the sample surface as prepared (left panel) and after immersion in 0.1 M KOH at +0.6 $V_{Ag/AgCl}$ (right panel).